Colloids and Surfaces A: Physicochemical and Engineering Aspects 681 (2024) 132725

Contents lists available at ScienceDirect

Colloids and Surfaces A: Physicochemical and Engineering Aspects

journal homepage: www.elsevier.com/locate/colsurfa

High-performance detection of trace chromium (VI) concentration by differential modulation fiber sensing system combining methimazole functionalized microfiber and fiber Bragg grating

Kang Sun [a], Chenfei Ma [a], Guoquan Wang [a], Lili Liang [b], Jizhou Wu [a,c], Dandan Sun [a,*], Jie Ma [a,c,**]

[a] School of Physics and Electronic Engineering, Shanxi University, Taiyuan, China
[b] Hebei key Laboratory of Optical Fiber Biosensing and Communication Devices, Institute of Information Technology, Handan University, Handan 056005, China
[c] Collaborative Innovation Center of Extreme Optics, Shanxi University, Taiyuan, China

GRAPHICAL ABSTRACT

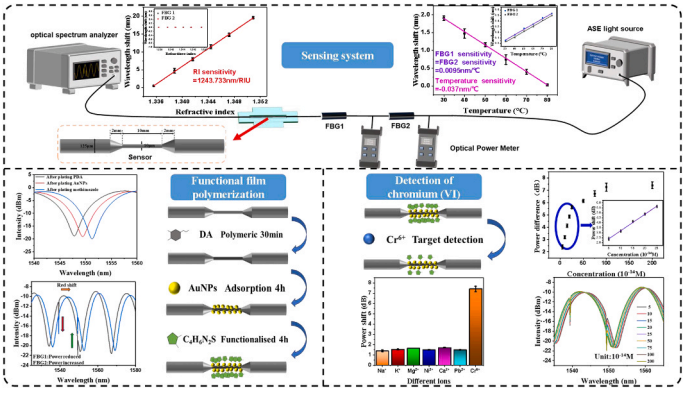

ARTICLE INFO

Keywords:
Microfiber
Fiber Bragg grating
Chromium (VI) ion detection
Differential modulation
Sensing system

ABSTRACT

In this paper, a sensing system based on the combination of methimethazole functionalized microfiber and fiber Bragg grating (FBG) is proposed for the monitoring of heavy metal ion - chromium (VI) ion (Cr^{6+}) in domestic water. The reaction of methimazole with Cr^{6+} under acidic conditions detachs methimazole from the microfiber, which affecting the surface refractive index and causing wavelength shift of the interference spectrum. The experimental results of Cr^{6+} detection in tap water show that the sensor has obvious response to Cr^{6+} in the concentration range of 5×10^{-14}-2×10^{-12} M, and the sensitivity is as high as -6.6×10^{12} nm/M in the concentration range of 5×10^{-14}-2.5×10^{-13} M with the detection limit of 2.7×10^{-15} M. Moreover, the differential modulation is used in the sensing system to detect Cr^{6+} through power change of FBG, which improves the sensitivity of the sensor and realizes lower detection limit and detection cost. The optimized sensitivity and detection limit by differential modulation are 1.53×10^{13} dB/M and 1.3×10^{-14} M, respectively.

* Corresponding author.
** Corresponding author at: School of Physics and Electronic Engineering, Shanxi University, Taiyuan, China.
E-mail addresses: sundd@sxu.edu.cn (D. Sun), mj@sxu.edu.cn (J. Ma).

https://doi.org/10.1016/j.colsurfa.2023.132725
Received 20 August 2023; Received in revised form 16 October 2023; Accepted 3 November 2023
Available online 4 November 2023

Therefore, this sensing system has high sensitivity, good selectivity and stability, and has a good application prospect in chromium (VI) ion detection.

1. Introduction

More than two centuries of urbanization and industrialization have produced a large amount of waste gas and waste water, which has brought a huge burden on the environment. In these emissions, heavy metals are harmful to the environment due to their high atomic mass and biological toxicity, and can be transferred to the human body through bioaccumulation, and can cause death in severe cases, which has caused extensive research [1–4]. Thus, heavy metal pollution is a major environmental problem that endangers public health. Heavy metals, such as lead (Pb), mercury (Hg), cadmium (Cd), chromium (Cr) and arsenic (As), have attracted much attention due to their high toxicity, prevalence and persistence in the environment [3]. Among them, chromium exists in the form of oxidized trivalent chromium (Cr^{3+}) and hexavalent chromium (Cr^{6+}) in the natural environment. Cr^{3+} is an element required for life, but Cr^{6+} is seriously life-threatening [2]. So it is necessary to design a high-sensitivity sensor for detecting Cr^{6+} to monitor the chromium ion content in industrial wastewater and domestic water.

At present, the reported methods for Cr^{6+} detection include normalization method [5], electrochemical method [6], spectroscopic method [7–9], chemical method [10], chromatography method [11,12], fluorescence method [13], etc. However, some of these methods have problems such as low sensitivity, long-time detection, and complex production. Therefore, it is required to propose a sensor with simple fabrication, high sensitivity and fast response to detect Cr^{6+} in water. Optic-fiber sensing is a relatively mature discipline, with its origins dating back to the mid-1970s [14]. Optic-fiber sensors have been widely used in many fields due to their advantages of small size, light weight, easy to use, and anti-interference. Since these sensors can operate in harsh conditions such as radiation environments, high pressures, and extreme temperatures, they have great application prospects in the aerospace field, marine sensing and object concentration [14,15].

In recent years, some optic-fiber sensors for chromium ion detection have also been reported. Castillo et al. developed an optical sensor for Cr^{6+} monitoring in industrial process water [16]; Yousefi et al. reported selective and sensitive speciation analysis of Cr^{6+} and Cr^{3+} in water samples by fiber optic-linear array detection spectrophotometry [17]; Kishore et al. designed a hydrogel-coated fiber Bragg grating to detect trace Cr^{6+} [18]; Long et al. proposed a novel surface-enhanced Raman scatting fiber probe modified with bifunctional methimazole for Cr^{6+} detection [19]; Wankar et al. reported a fiber optic sensor for selective determination of Cr^{6+} using diffuse reflection spectroscopy [20]; Menon et al. fabricated a fiber optic sensor for Cr^{6+} detection based on a metal-organic framework [21]. The above sensors have made great achievements in the field of chromium ion detection, but some of them also have problems such as complex fabrication and high cost. Because of its advantages of simple fabrication, low cost and high sensitivity, the tapered microfiber interferometer solves the above problems and has obvious advantages in detecting ion concentration [22,23]. In recent years, there have been many studies on the application of microfiber interferometer for ion detection. For example, Yap et al. (2018) reported a hand-held microfiber sensor modified with L-glutathione for ultra-sensitive lead ion detection [24]. Yi et al. reported a microfiber sensor coated an imprinting template for detecting nickel ions [25]. Wang et al. fabricated a polydopamine-maleic acid coated microfiber sensor for trace detection of lead ions [26]. These reported microfiber sensors are combined with functional membranes that can react specifically with the measured object to improve sensor sensitivity and specificity.

Optical sensors or optical probes detect ions, proteins or other substances, and the detection results are mainly reflected by the intensity change of the spectrum or the shift of the spectrum [27]. For example, Xiao et al. developed a highly specific detection immune sensor based on Hi-Bi μFBG [28]; Also Ran et al. proposed a fiber interstitial needle carrying hypoxia-sensitive fluorescent probes for use in endoscopic cancer sensing [29], both of which reflect the detection results by changes in the intensity of the spectrum. However, the sensitivity of this method is not high enough, and the detection limit is limited. Hou (2023) developed a fiber microfiber biosensor based on β-cyclodextrin, which reflects the detection results through the movement of the spectrum [30]. However, the detection results of this method are not intuitive enough, and the cost of the instrument is high. Zhang et al. designed a differential intensity modulated refractive index sensor consisting of a coreless fiber filter with the RI sensitivity of − 99.191 dB/RIU and − 139.958 dB/RIU at the range of 1.3329–1.3781 and 1.3781–1.401, respectively [31]. Based on the above discussion, a differential intensity modulated sensing system converted into the power change of fiber grating has a relatively large advantage of intuitive result, improved sensitivity and low instrument cost.

In this paper, a differential modulation optical fiber sensing system combining methylimidazole functional microfiber interferometer and fiber grating is designed for the efficient detection of trace chromium (VI) concentration. Functionalization of microfiber using methimazole is due to the specific redox reaction between methimazole and Cr^{6+} ions [32]. When the subsequent sensor detects the tap water sample, experimental analysis shows that the sensor has a significant response when the chromium ion concentration ranges from 5×10^{-14} M to 2×10^{-12} M. In the low concentration range (5×10^{-14} M to 2.5×10^{-13} M), the sensor sensitivity is as high as -6.6×10^{12} nm/M and the detection limit is 2.7×10^{-15} M. Because the central wavelength of FBG is not affected by the external refractive index, so the change of the microfiber interference spectrum will be reflected in the change of FBG power, which can increase the detection sensitivity and reduce the detection limit. The experimental results show that the higher sensitivity of 1.53×10^{13} dB/M and the lower detection limit of 1.3×10^{-14} M can be obtained by relying on the power difference of FBGs. A cheaper and smaller device-power meter can be used to replace the spectrometer to observe the response Cr^{6+} concentration, thus reducing the cost and volume of the sensing system and making the detection results more intuitive [33]. Moreover, the sensor has good selectivity for chromium ions, and the effect of detecting chromium ions in tap water is good. Therefore, the proposed sensor has a positive significance for the analysis of Cr^{6+} concentration in the water environment and the monitoring and protection of water quality.

2. Experiment procedure

2.1. Reagents and instruments

Chloroauric acid (HAuCl4), Sodium borohydride (NaBH4), Dopamine hydrochloride (DA, 98 %),tromethane hydrochloride buffer (Tris-HCl, 1.0 M, pH8.5),2-Mercapto-1-methylimidazole ($C_4H_6N_2S$, 98 %), Acetic acid (AR, 99.5 %), potassium dichromate solution ($K_2Cr_2O_7$, 0.0999 mol/L, medium: H_2O),Calcium chloride anhydrous ($CaCl_2$, 99.99 %), Nickel(II) chloride (Cl_2Ni, 99 %), Lead chloride ($PbCl_2$, 99.99 %),Magnesium chloride ($MgCl_2$,99.9), Potassium chloride (KCl,99.8 %) and Sodium chloride (NaCl, 99.5 %) were purchased from Shanghai Macklin Biochemical Technology Co., ltd. (Shanghai, China). AuNP was prepared by reducing HAuCl4 and NaBH4. DA dissolved in Tris-HCl buffer. 2-Mercapto-1-methylimidazole and heavy metals dissolved and diluted in deionised water (DI).

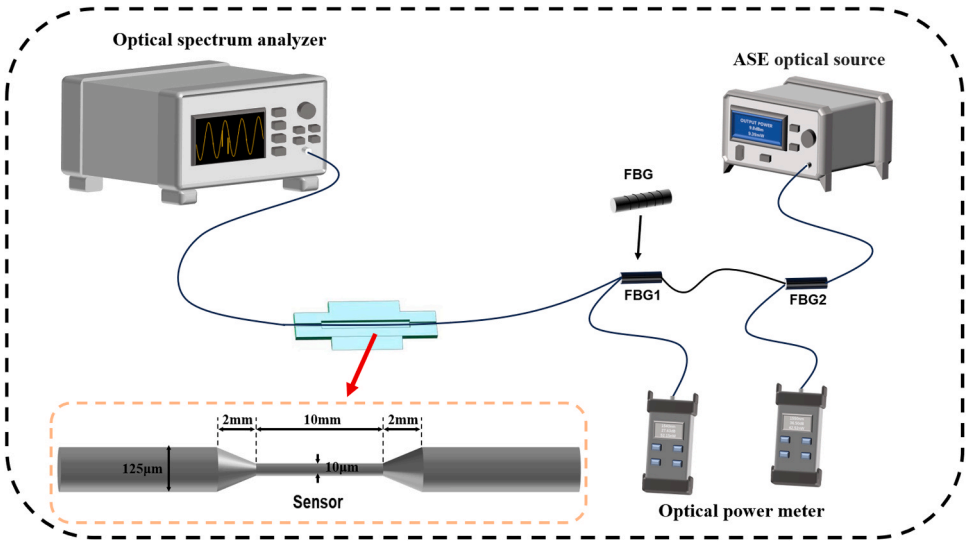

Fig. 1. Schematic diagram of optical fiber sensing system and structure of microfiber interferometer with parameters.

Instruments used during the experimental tests include an amplified spontaneous emission (ASE)optical source, an optical spectrum analyzer (OSA, YOKOGAWA, AQ6370C, Japan) and two optical power meters. The equipment used in the preparation of optic-microfiber sensor are optical fiber fusion splicer (Fujikura FSM-60S, Japan), motion controller (Zolix, MC600, China). In addition, in subsequent experiments, the instruments for the preparation of sample solutions used are pH meters (PHS-3E, INESA, China), digital refractometer (AR200, Reichert, America) and column heater (HT-230A, China). Finally, the instruments used in the characterization are scanning electron microscopy (SEM, Zeiss Sigma HD, Germany), and the energy dispersive spectrometer (EDS, Zeiss Sigma HD, Germany).

2.2. Experimental setup

The experimental setup of the whole experiment is shown in Fig. 1. Light in the wavelength range 1528–1603 nm (output power of 10 dBm) is emitted from the ASE light source, passed through the fabricated microfiber interferometer, formed the interferometric spectrum, and finally detected by the OSA (600–1700 nm) with a resolution of 0.02 nm. Two Fiber Bragg Gratings (FBGs) are connected through fiber circulators to two optical power meters, which monitor the power of the grating. The microfiber interferometer is placed in a special groove with a width of 5 mm in the center and 2 mm on the sides and a depth of 2 mm, which ensures that the microfiber interferometer can be completely submerged in the measured solution and that the groove structure protects the measured solution from escaping.

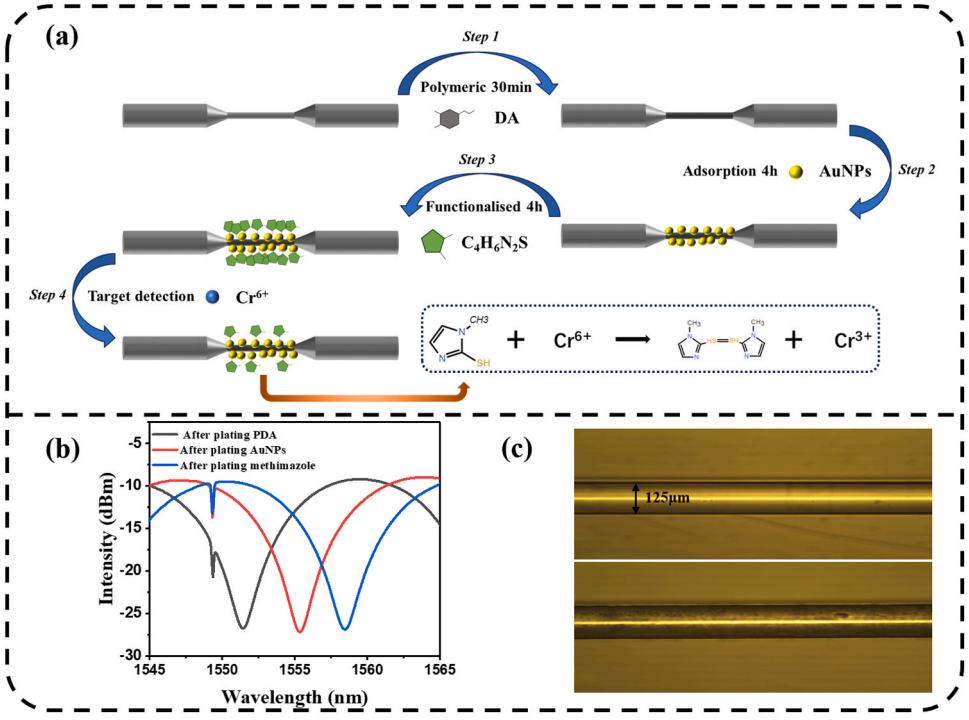

Fig. 2. (a) Schematic diagram of functional microfiber detection of Cr^{6+} concentration; (b) Schematic diagram of functional microfiber interference change; (c) The single-mode fiber metallographic microscope images before and after functionalization.

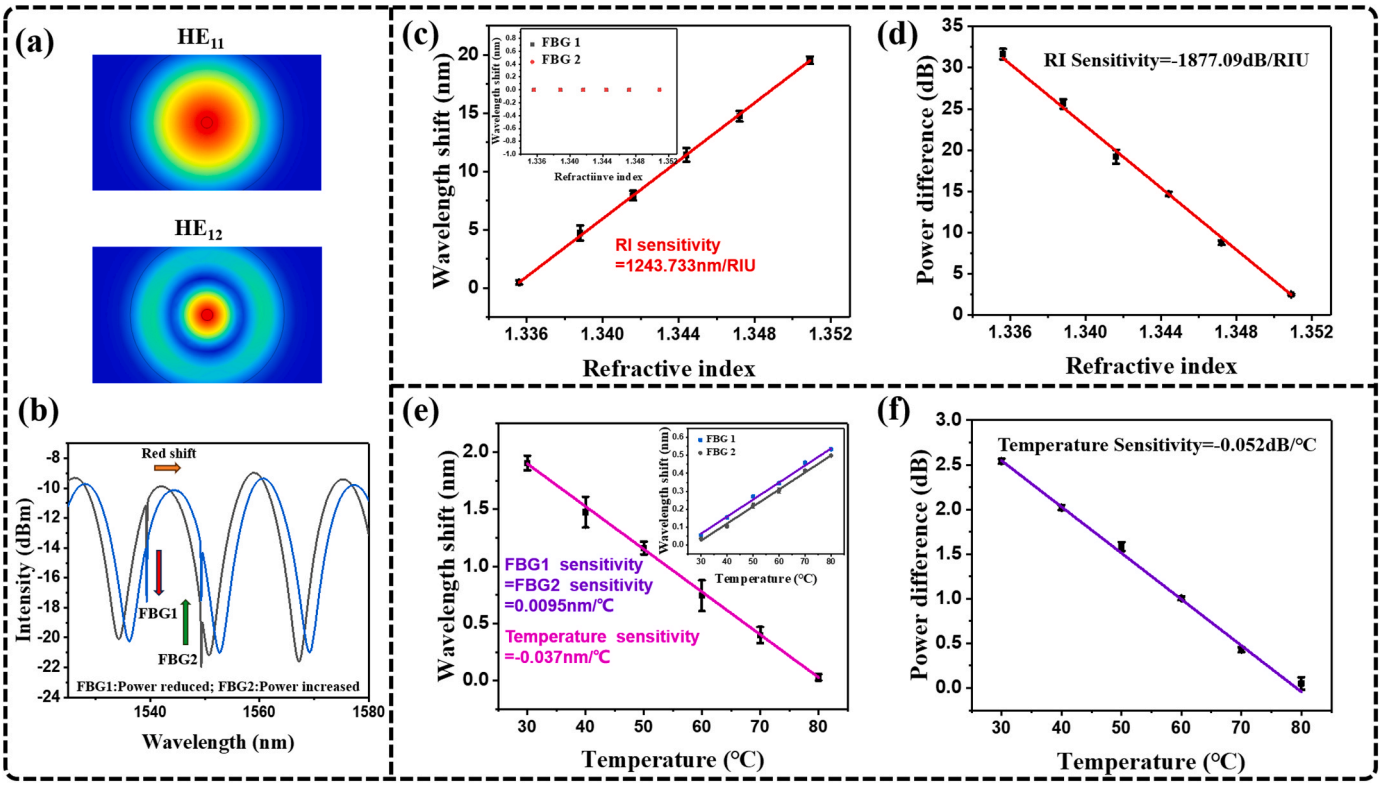

Fig. 3. (a) Two models of HE_{11} and HE_{12} in microfiber; (b) Schematic diagram of microfiber and FBG working principle; (c) The relationship between the external RI change and the spectral wavelength change of microfiber interferometer and FBG; (d) The corresponding relationship between the external RI and power difference; (e) The relationship between temperature and the spectral wavelength change of microfiber interferometer and FBG; (f) The corresponding relationship between temperature and power difference.

2.3. Fabrication of sensors

Firstly,The manufacture procedure of the microfiber interferometer is as follows: a section of germanium-doped silicon fiber of 2–3 cm is fused in the middle of the single-mode fiber with a fiber fusion splicer, and after being heated by a high-temperature spitfire gun for 5 s, this section of the fiber is uniformly stretched by 14 mm with a motion controller, and the resulting microfiber interferometer is shown in the dashed box in Fig. 1, which consists of two conical transition regions with a length of 2 mm and a uniform region with a length of 10 mm and a diameter of 10 μm.

The next step is to functionalize the microfiber interferometer. The principle is as follows: the polymerization of dopamine to the surface of microfibers depends on its strong adhesion and physical adsorption to the surface of microfibers [34]. Due to its adhesion and abundant active groups, polydopamine coating can be functionalized with metal nanoparticles and polymers, etc., so polymerization on the surface of objects to produce “polydopamine film” has become a popular and simple coating method [35]. The adsorption of gold nanoparticles is due to the in-situ reduction of gold nanoparticles through the amino group and catecholyl group of the generated PDA film. Moreover, the PDA membrane is a nanoporous membrane, which also provides attachment points for the adsorption of gold particles [36]. Finally, the adhesion of methimazole is due to the sulfhydryl groups on the methimazole, and the gold nanoparticles adsorb methimazole through Au-S covalent bonds [37].

The process of functionalization is the first three steps in Fig. 2(a). In the step 1, the microfiber interferometer is immersed in a configured 0.5 g/mL dopamine solution for 30 min, and then washes and dries with DI. In the step 2, the dopamine-treated microfiber interferometer is immersed in AuNPs solution for 4 h, and then washes and dries again. In the step 3, the microfiber interferometer is immersed in 0.5 M mercaptoimidazole solution for 2 h, and then washes and dries to obtain the functional microfiber interferometer sensor. Step 4 in Fig. 2 (a) shows the detection of hexavalent chromium ions by this functional microfiber interferometer sensor, and the change in the spectrum after functionalizeing the microfiber interferometer was shown in Fig. 2 (b). Fig. 2(c) shows the metallographic micrograph of the single-mode fiber before and after functionalization. The detection principle is shown in the dotted box in Fig. 3. Under acidic conditions, hexavalent chromium can react with methimazole in a redox reaction destroying the sulfhydryl group (-SH) connecting the methimazole to the gold particles, and the methimazole will detach from the microfiber interferometer, leading to a change in the refractive index of the surface of the microfiber interferometer and a blueshift in the spectrum.

3. Results and discussion

3.1. Sensing principles and mechanism

The schematic diagram of microfiber in the dashed box in Fig. 1 is shown, the microfiber is divided into two conical transition regions and a uniform region of the waist. When the light passes through the first conical transition region, the core fundamental mode (HE_{11}) is excited and coupled to the cladding mode (HE_{12}) [38]. The two modes of HE_{11} and HE_{12} in the manufactured microfiber are shown in Fig. 3 (a). After the two modes pass through the uniform region of the waist, they are re-coupled to the single-mode fiber transmission in the rear conical region, resulting in the appearance of interference wavelengths. Due to the difference in effective refractive index between the core mode and the cladding mode, a Mach-Zehnder interferometer is formed [39]. φ is the phase difference between the two modes, namely [40]:

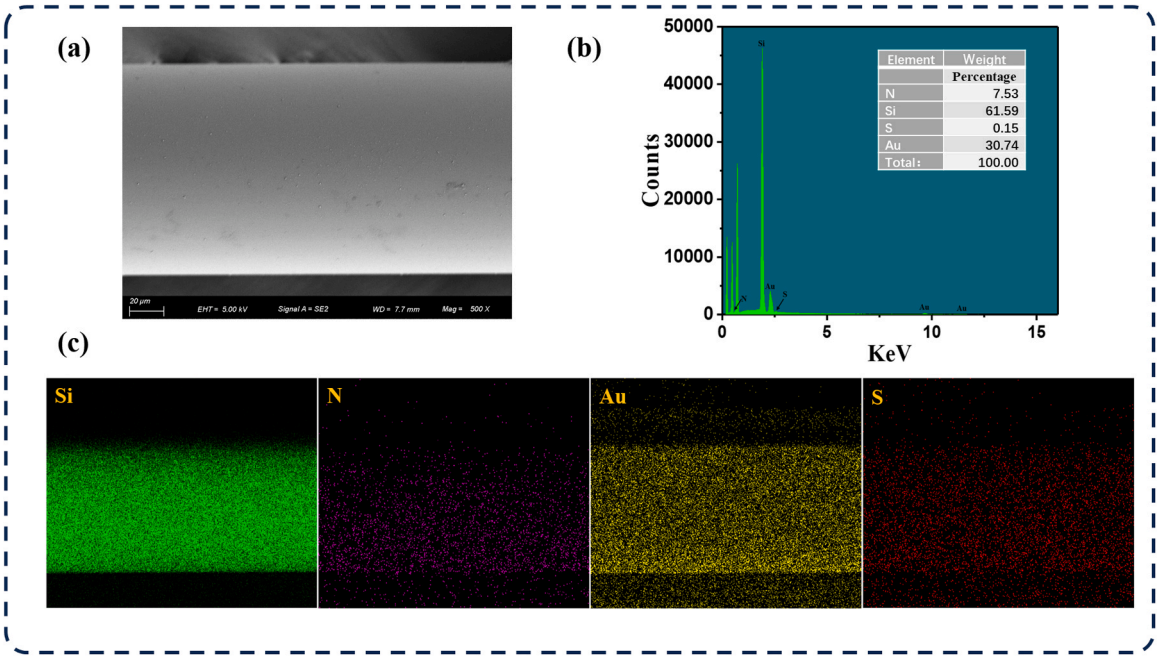

Fig. 4. (a) SEM characterization of functional fibers; (b) EDX analysis (the inserted table is element content analysis) (c) Mapping analysis.

$$\varphi = \frac{2\pi}{\lambda}\Delta n_{eff} L \tag{1}$$

where λ is the central wavelength of the transmitted light, Δn_{eff} is the difference of the effective refractive index between the two modes, and L is the length of the waist uniform region of the microfiber. If the external refractive index of the microfiber changes, the difference of the effective refractive index between the two modes will also change, and it can be seen from the Formula (1) that the phase difference between the two modes will also change, resulting in the change of the interference spectrum. To further understand the sensitivity of RI, the spectral response of the external RI can be obtained by taking a small n_{SRI} change from Formula (1), which considers φ to be constant. After a few mathematical crunches, we get [41]:

$$S = \frac{d_\lambda}{d_{n_{SRI}}} = \frac{\lambda}{G}\left(\frac{\partial \Delta n_{eff}}{\partial n_{SRI}}\right) \tag{2}$$

where n_{SRI} is the external refractive index, $G = \Delta n_{eff} - \lambda\partial(\Delta n_{eff})/\partial\lambda$ is the group effective refractive index difference between the HE_{11} mode and the HE_{12} mode, which is usually negative in microfibers [42], and $\partial\Delta n_{eff}/\partial n_{SRI}$ is an index-dependent change caused by RI. According to Formula (2), the refractive index sensitivity of microfiber is determined by G, λ, and $\partial\Delta n_{eff}/\partial n_{SRI}$. When the external refractive index changes, the change in Δn_{eff} is smaller than the change in ∂n_{SRI}, so $\partial\Delta n_{eff}/\partial n_{SRI}$ is negative and S is positive. Therefore, the increase of external RI will cause the redshift of interference spectrum. The finite element method is used to numerically simulate the microfiber, and the refractive index sensitivity is calculated to be 1060.005 nm/RIU, which was very close to the experimental results. During the process of microfiber functionalization, the surface refractive index of microfiber increases the interference spectrum redshift. In the process of detection, the surface refractive index of the microfiber decreases due to the removal of methimazole from the surface, and the interference spectrum blueshifts. Moreover, due to the ultra-small diameter of microfibers, which provides a stronger evanescent field, microfiber interferometer has higher RI sensitivity.

When the light is transmitted to the grating, only the light that meets the condition of Bragg's central wavelength will be reflected, and the rest of the wavelength will be transmitted through the grating [43,44], whose central wavelength is:

$$\lambda_1 = 2n_1\wedge \tag{3}$$

where n_1 is the effective refractive index of fiber Bragg grating, and $\wedge$ is the period length. The central wavelength is determined by these two parameters, and the change of the central wavelength of the Bragg fiber grating can be expressed by the following Formula (3). When external physical quantities such as temperature, stress and pressure change, the effective refractive index and grating period of FBG will also change, resulting in changes in the central wavelength. However, in FBG, the incident and reflected transmission modes are coupled in the fiber core, and only a small part can interact with the external medium through the cladding, thus FBG is almost unaffected by the environmental refractive index [45].

3.2. Basic sensing performance

The effects of refractive index and temperature on microfiber interferometer and fiber grating are studied experimentally. The refractive index solution used in the experiment is obtained by configuring NaCl and DI. The instruments are digital refractometer to measure the refractive index and column heater to control the temperature. The refractive index measured in the experiment ranged from 1.3356 to 1.3509, and the temperature ranged from 30 ℃ to 80 ℃. When the external refractive index changes, the interference spectrum of the microfiber will also change, as shown in Fig. 3 (b). However, the central wavelength of FBG is unchanged, so the change of grating spectral shape is manifested as the change of power in Fig. 3 (b). In the subsequent detection, the change of microfiber spectrum can be seen through this difference. Fig. 3 (c) shows the relationship between the external RI change and the change of spectral wavelength of microfiber interferometer and grating, which is consistent with the above theoretical analysis. The change of refractive index has no effect on the central wavelength of FBG, and the wavelength shift RI sensitivity of microfiber is 1243.733 nm/RIU. The corresponding relationship between the external RI and power difference is shown in Fig. 3 (d), and the power difference RI sensitivity is − 1877.09 dB/RIU. Fig. 3 (e) and Fig. 3 (f) show the corresponding relationship between temperature and microfiber interferometer and FBG. The temperature sensitivity of microfiber interferometer is − 0.037 nm/℃, the temperature sensitivity FBGs is

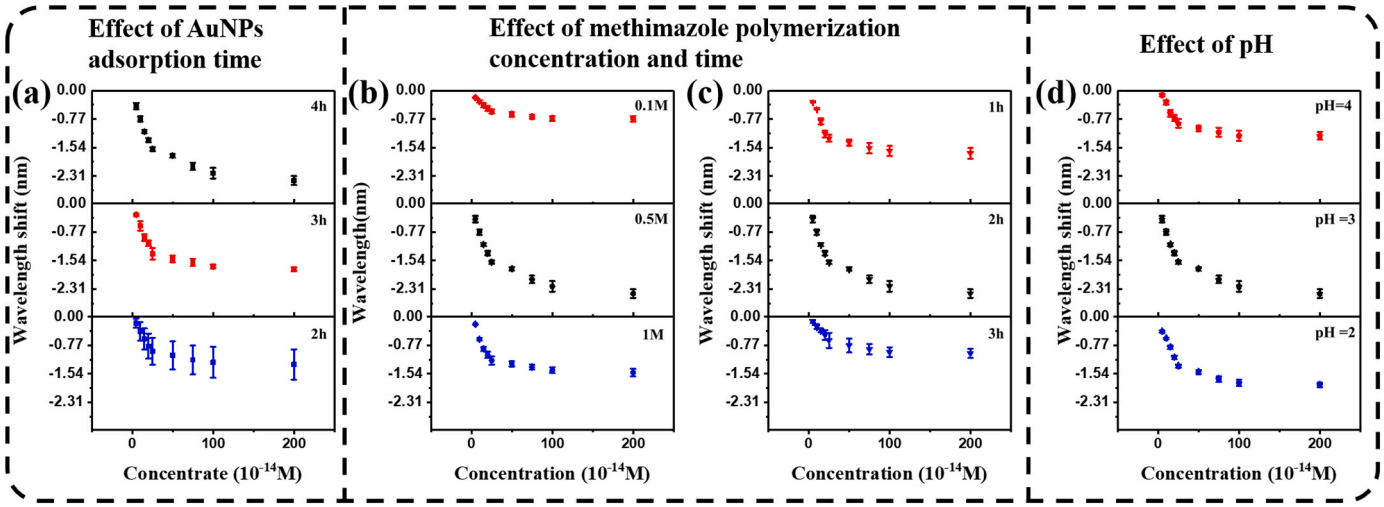

Fig. 5. (a) Response of functional sensing probe to chromium ion detection under different times of AuNPs immersion; (b) Response of different methimazole concentrations to chromium ion detection; (c) Response to chromium ions under different times of attached methimazole; (d) Detection response of chromium ions at different pH.

0.0095 nm/℃ and the sensitivity between power difference of FBGs and temperature is − 0.0052 dB/℃.

3.3. Characterization of microfiber interferometer

In order to confirm that the microfiber interferometer is coated by the film, the surface morphology and chemical composition of the fiber are analyzed by SEM and EDX spectroscopy. Fig. 4 (a) is SEM image of the fiber surface after functionalization, which shows the functionalized uniform film on the fiber surface. Fig. 4 (b) shows the analysis results of elements on the surface of the optical fiber, where Si element is the component element of the optical fiber, N element comes from PDA and methimazole, Au proves the successful adhesion of gold particle AuNPs, and S proves the successful adhesion of methimazole. The black of the optical fiber under metallographic microscope in Fig. 2 (c) proves the adhesion of melanin PDA. In Fig. 4 (c), the mapping analysis of corresponding Si, N, Au and S elements. From the above experimental analysis, it can be concluded that the microfiber interferometer is successfully functionalized by PDA, gold particles and methimazole.

3.4. The functionalization of microfiber interferometer

The attachment of nanofunctional membrane to microfibers is an important step in the preparation of sensors. PDA, gold particles and methimazole are attached to the microfiber in three steps by dipping coating method described in Section 2.3. We further study the influence of gold particle attachment time, methimazole immersion time and methimazole concentration on the subsequent detection of chromium ions. In addition, because the redox reaction of methimazole and Cr (VI) needs to be under acidic conditions, the influence of the pH of chromium ion solution on the detection of chromium ions is further studied. In order to determine various parameters of the optimal functionalization of microfibers, comparative tests are carried out, and the results of the comparative experiments with error bars are shown in Fig. 5.

Fig. 5 (a) shows the results of comparative experiments with different gold plating times during the functionalization process. Three microfiber interferometers coated on PDA are immersed in AuNPs solution for 2 h, 3 h, and 4 h, respectively; after washing and drying. The functionalization of microfiber interferometer after immersing in 0.5 M methimazole for 2 h detects the different concentration of Cr^{6+} (5,10,15,20,25,50,75,100,200 (unit 10^{-14} M)). In Fig. 4 (a), with the increase of gold plating time, the sensitivity of the sensor to detect chromium ions increases. The blue shift of the interference spectrum is 2.52 nm, which is higher at 2 h than at 1.58 nm and at 3 h than at 1.81 nm. Thus, 4 h is selected as the time of dipping gold particles. The reason for this result may be that as the adsorption time of gold particles increases, the more gold particles are adsorbed on the surface of microfibers, which makes more binding points for the subsequent functionalization of methimazole on the microfiber.

Fig. 5 (b) and (c) shows the results of concentration and the dipping time of methimazole in the process of functionalization of microfiber interferometer. Three identical microfiber interferometers coated on PDA/AuNPs are immersed in methimazole solution at the concentrations of 0.1 M, 0.5 M and 1 M for 2 h. In Fig. 5(b), the experimental effect is better when 0.5 M methimazole is plated, and the blue shift of the interference spectrum is the most obvious, reaching 2.52 nm, which is higher than the rest of 1.58 nm and 0.82 nm. Thus, it is better to select 0.5 M methimazole. Fig. 5 (c) shows the results of comparative tests functionalized with 0.5 M methimazole for different times. The process of this comparative test is the same as the previous comparative test of different concentrations of methimazole, except that functionalized methimazole is used at the same concentration of 0.5 M and different time periods of 1 h, 2 h and 3 h. It can be seen from the experimental results that the blue shift amplitude of the interference spectrum at 2 h is the largest, reaching 2.52 nm, while 1 h and 3 h only have 1.08 nm and 1.82 nm.

After the conditions for the optimal functionalization of the microfibers are determined, three sets of comparative tests are also performed on the pH of the chromium ion solution. The comparative experimental results are shown in Fig. 5 (d). The production process of three functionalized microfiber interferometers is similar to that of the comparison experiment above to adopt the optimal functionalization time and concentration. The fabricated sensors are used to detect chromium ion solutions with pH of 2, 3, and 4, respectively. From the experimental results of Fig. 5 (d), the detection effect is best at pH 3, and the blue shift of the interference spectrum is 2.52 nm, which is larger than the 1.88 nm and 1.33 nm at pH 2 and pH 4. Based on the above studies, we finally adopt the adsorption time of gold particles for 4 h, the immersion time of methimazole for 2 h, the concentration of methimazole for 0.5 M, and the pH of detecting chromium ions at 3.

3.5. Detection of chromium ion (Cr^{6+})

Based on the principle of detection Cr^{6+} described in previous Section 2.3, in an acidic environment, the hexavalent chromium ion reacts with methimazole, causing it to fall off the sensor surface, thus resulting

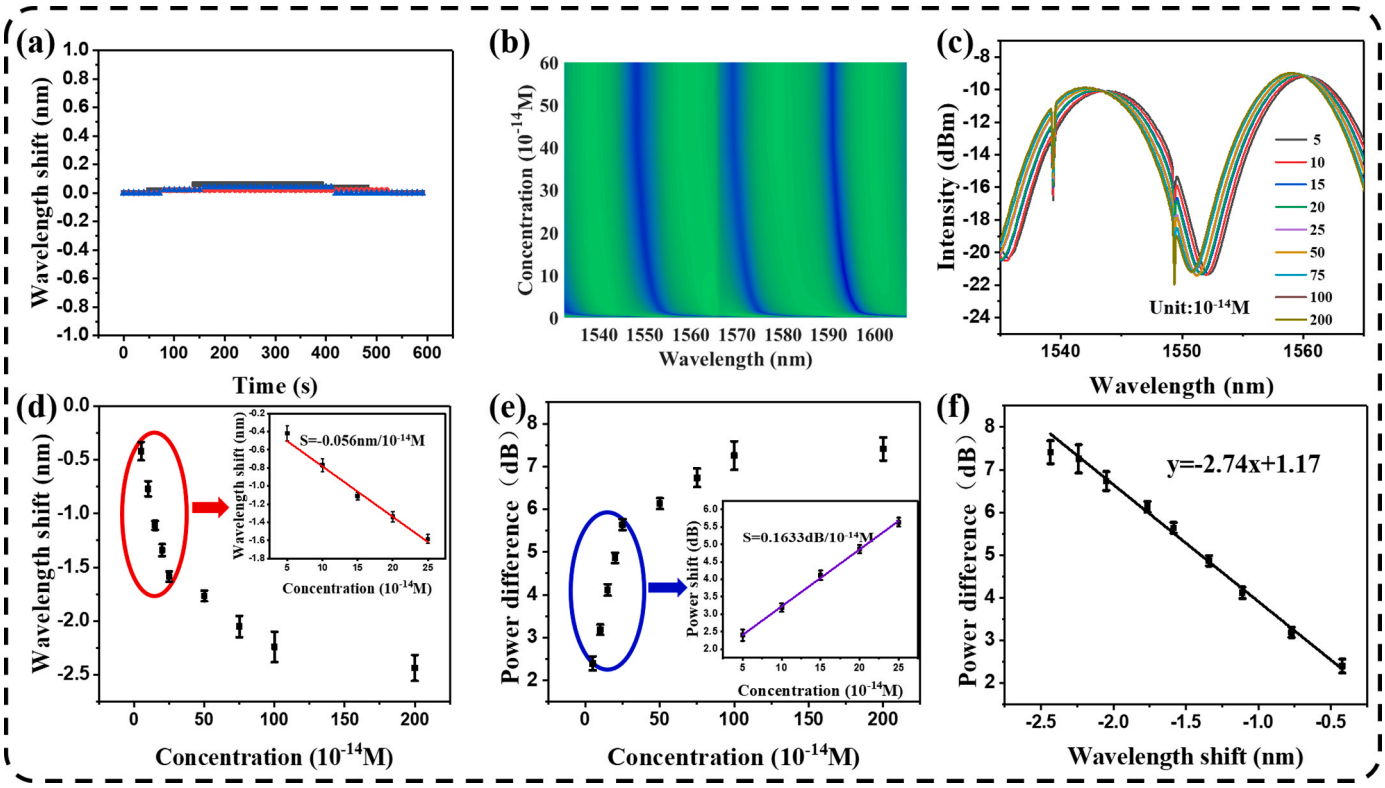

Fig. 6. (a) The wavelength shift by recording the spectrum of functional sensing probe in three times of deionized water; (b) The interference spectral wavelength response of Cr^{6+} concentration was measured by a functional sensor probe; (c) The shift of the corresponding interference spectrum; (d) Response of sensor wavelength drift to Cr^{6+} in the range of 5×10^{-14} M to 2×10^{-12} M; (e) The response of the power difference to Cr^{6+} in the range 5×10^{-14} M to 2×10^{-12} M; (f) The corresponding relationship between wavelength shift and power difference.

in a blue shift in the interference spectrum and an increase in the power meter difference. Before the detection of chromium ions, the sensor is washed with DI solution, and the results of three times are shown in Fig. 6 (a). The maximum spectral shift with water washing is 0.06 nm, and the results show that the sensor fabricated after DI washing is stable.

The sensor fabricated in Section 2.3 detects various concentration of chromium ions sequentially from low concentration to high concentration. Chromium ions are dissolved and diluted with DI, and adjusted to pH 3 with acetic acid. Fig. 6 (b) shows the wavelength response of the interference spectrum, from which the wavelength blue-shift trend during the detecting process. Fig. 6 (c) shows the specific interference spectra of different concentrations of chromium ions. It can be clearly seen that as the chromium ion concentration increases, the interference spectrum shifts to the left and the power changes. Fig. 6 (d) shows the error bar fitting plot of the corresponding relationship between chromium ion concentration and wavelength shift in three experiments. In the low concentration range of 5×10^{-14} M to 2.5×10^{-13} M, the results show a good linear relationship with a detection sensitivity of -5.6×10^{12} nm/M, as shown in the inset of a magnified Fig. 6 (d). The correspondence between the power difference and the chromium ion concentration is shown in Fig. 6 (e). There is a good linear relationship between the power difference and the low concentration range (5×10^{-14} M-2.5×10^{-13} M) of chromium ions with the detection sensitivity of 1.633×10^{13} dB/M, as shown in the inset of Fig. 6 (e). Fig. 6 (f) shows the correspondence between the power meter and the wavelength drift during the detection process. The overall linear

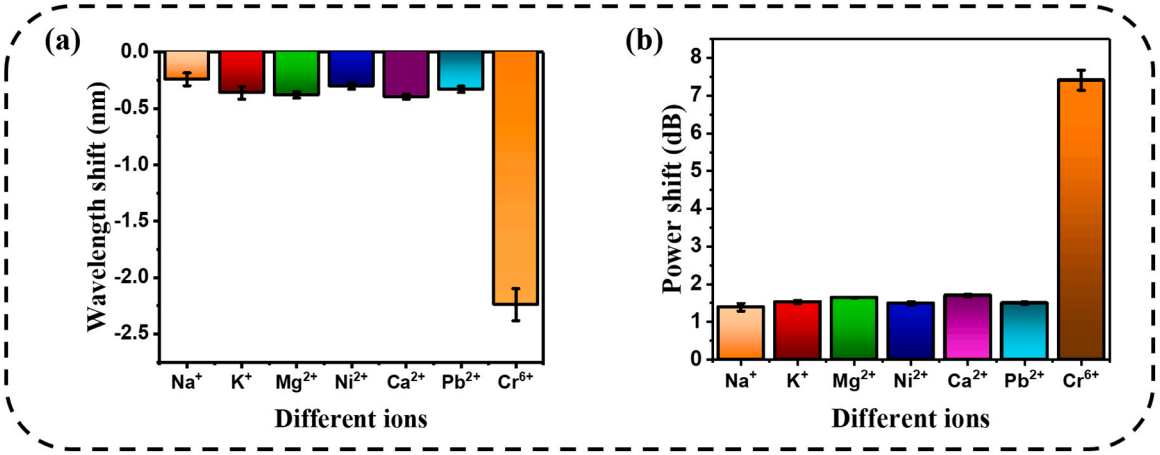

Fig. 7. (a) Wavelength drift detected by the sensor for different ions (b) Power difference detected by the sensor for different ions.

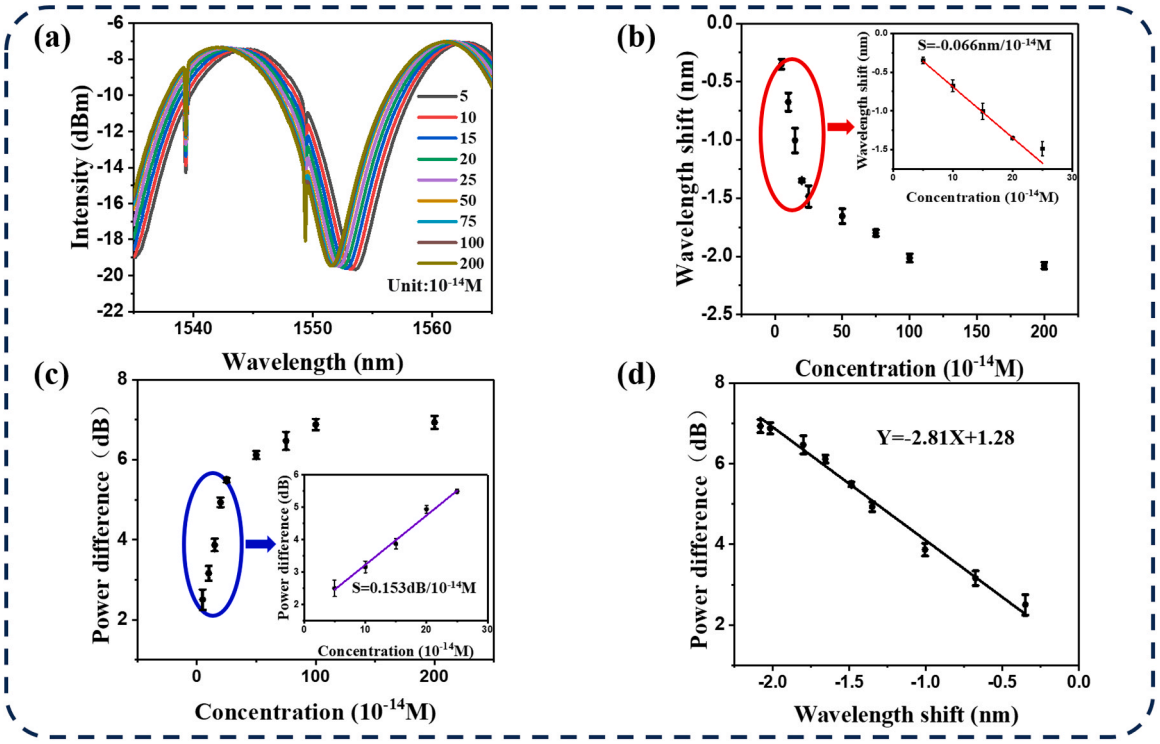

Fig. 8. The detected results of chromium ion solution diluted by tap water. (a) The shift of the corresponding interference spectrum; (b) Response of sensor wavelength drift to Cr^{6+} in the range of 5×10^{-14} M to 2×10^{-12} M; (c) The response of the power difference to Cr^{6+} in the range 5×10^{-14} M to 2×10^{-12} M; (d) The corresponding relationship between wavelength shift and power difference.

relationship is good with the corresponding linear equation of $y = -2.74x + 1.17$. The theoretical detection limit of the interference spectrum wavelength shift for chromium ions can be calculated by the formula $LOD_1 = 3\sigma_1/S_1$, where $\sigma_1 = 0.06$ nm is the standard deviation of the measurement error, $S_1 = -5 \times 10^{12}$ nm/M is the slope of the fitting curve, and the LOD_1 is 8.45×10^{-15} M. Similarly, if the measurement standard error of the power difference σ_2 is 0.07 dB and the slope of the fitting curve S_2 is 1.633×10^{13} dB/M, the theoretical detection limit for chromium ions can be calculated as 4.2×10^{-15} M. These two detection limits are far lower than the standard of hexavalent chromium ion in domestic water (1×10^{-7} M) stipulated by the World Health Organization. According to the above experimental results and analysis, the methimazole functionalized sensor has good stability, high detection accuracy and good repeatability for hexavalent chromium ions.

3.6. Selectivity of sensor

To verify the specific response of the sensor to hexavalent chromium ions, the fabricated sensor is used to detect several ionic solutions of Na^+, K^+, Mg^{2+}, Ni^{2+}, Ca^{2+} and Pb^{2+} at concentration of 10^{-12} M prepared with DI and adjusted to pH 3 with acetic acid. Fig. 7 (a) shows the wavelength drift map of the interference spectrum for detecting different ions by the sensor. The wavelength shift of chromium ion is 2.52 nm, which is much higher than that of other ions, and the wavelength shift of other ions is 0.24 nm for sodium ion, 0.36 nm for potassium ion, 0.38 nm for magnesium ion, 0.3 nm for nickel ion, 0.39 nm for calcium ion and 0.33 nm for lead ion. Fig. 7 (b) shows the response of power difference of FBGs for different ions. Consistent with the wavelength shift result, the power difference for chromium ions (7.42 dB) is also much larger than for the other ions, which are 1.39 dB for sodium ions, 1.53 dB for potassium ions, 1.64 dB for magnesium ions, 1.49 dB for nickel ions, 1.7 dB for calcium ions, and 1.5 dB for lead ions, respectively. It can be seen from the experimental results that the sensor has good selectivity for hexavalent chromium ions, because of the strong oxidation of hexavalent chromium ions to oxiditize methimazole into disulfide and reduce itself to trivalent chromium ions, which is not available for other metal ions. From the above experiments and analysis, it can be concluded that the fabricated sensor can specifically detect hexavalent chromium ions.

3.7. Detection of real samples

The prepared sensor is used to detect the chromium ion solution dissolved and diluted by tap water and the pH is adjusted to 3 by acetic acid. The detection results are shown in Fig. 8. Fig. 8 (a) shows the shift of the corresponding interference spectrum, which shows a trend of blue shift. Fig. 8 (b) shows the error bar diagram of the corresponding relationship between the chromium ion concentration and the wavelength shift of the interference spectrum in three experiments. As shown in the inset, there is a good linear relationship between the two in the range of low concentration (5×10^{-14} M-20×10^{-14} M), and the theoretical detection limit of wavelength drift of the interference spectrum is calculated by the formula $LOD_3 = 3\sigma_3/S_3$, where $\sigma_3 = \sigma_1 = 0.06$ nm, $S_3 = -6.6 \times 10^{12}$nm/M is the slope of the fitted curve, LOD_3 is calculated as 2.7×10^{-14} M. Fig. 8 (c) is the error bar diagram of the corresponding relationship between ion concentration and power difference of fiber grating. It can be seen from the insertion diagram of Fig. 8 (c) that the ion concentration and power difference have a good linear relationship in the range of concentration 5×10^{-14} M-2.5×10^{-13} M, and the sensitivity S_4 is calculated as 1.53×10^{13} dB/M. Similarly, $\sigma_4 = \sigma_2 = 0.07$ dB, so the detection limit is calculated as $LOD_4 = 1.3 \times 10^{-14}$ M. Fig. 8 (d) shows the corresponding relationship between wavelength drift and power difference during detection, and the fitted linear equation is $Y = -2.81X + 1.28$. According to the relationship, the concentration can be inferred from the power difference, thus the cost of the system can be saved and the volume can be reduced. From the experiments, it can be concluded that the proposed sensor can be used for hexavalent chromium ion detection in tap water.

Table 1
Comparison of different optic fiber sensors for Cr^{6+} detection.

Methods	Main chemical materials	Linear range	Sensitivity	detection limit	Manufacturing difficulty	Cost	Reference
Atomic absorption spectrophotometry	Raipore R1030 membrane, anion-exchange membrane containing ammonium groups as ionogenic groups	10^{-4}-3×10^{-4} M	-	10^{-3} M	Difficult	Medium	[16]
Spectrophotometry	1,5-diphenylcarbazide	4×10^{-9}-4×10^{-7} M	-	1×10^{-9} M	Difficult	Hight	[17]
Hydrogel coated FBG	3-arylamidopropyltrimethylammoniumchloride	2×10^{-7}-2×10^{-6} M	6×10^{4} nm/M	1.5×10^{-9} M	Easy	Medium	[18]
Surface-enhanced Raman scatting fiber probes	Methimazole/Ag^{+}	10^{-11}-10^{-5} M	-	10^{-11} M	Medium	Medium	[19]
Diffuse reflectance spectroscopy	1,5-diphenylcarbazide	2×10^{-7}-2×10^{-5} M	-	2×10^{-7} M	Difficult	Medium	[20]
U-shaped bent fiber based on metal-organic frame	zeolitic imidazolate	10^{-7}-2×10^{-3} M	-	2×10^{-8} M	Difficult	Medium	[21]
Tapered microfiber interferometer and FBG	Methimazole	5×10^{-14}-2×10^{-12} M	-5 $\times 10^{-12}$ nm/M 0.1633 dB/10^{-14} M	8.45×10^{-15} M 4.2×10^{-15} M	Easy	Low	This work

Table 1 compares the performance of the designed sensor with other fiber optic sensors for Cr^{6+} detection. As can be seen from the table, the sensor has a very high sensitivity and detection limit for Cr^{6+}, and is simple to manufacture and low cost. The device has good stability, anti-electromagnetic interference ability, flexibility and miniaturization required by the next generation of chromium ion detection technology, which has great advantages in the detection of Cr^{6+}.

4. Conclusion

This paper presents a fiber optic sensing system based on the combination of microfiber interferometer coated with methimazole functional membrane and FBG for monitoring Cr^{6+} in domestic water. The functional film is polymerized to the surface of the microfiber interferometer by dipping coating method. In the tap water detection, the sensor has obvious response to Cr^{6+} in the concentration range of 5×10^{-14}-2×10^{-12} M, and the sensitivity of -6.6×10^{12} nm/M in the concentration range of 5×10^{-14}-2.5×10^{-13} M with the detection limit of Cr^{6+} of 2.7×10^{-14} M. The sensing system realizes differential modulation through the power difference between two FBGs, which improves the sensitivity of the sensor, reduces the detection limit and detection cost. The optimal sensitivity of the optimized sensor is 1.53×10^{13} dB/M, and the detection limit is 1.3×10^{-14} M.The experimental results show that the detection limit of Cr^{6+} by the proposed sensor is much lower than the World Health Organization standard (1×10^{-7} M), and has good selectivity and stability. This a sensing system can meet the detection of Cr^{6+} concentration in most environments, and is of great significance for the detection of heavy metal pollution.

CRediT authorship contribution statement

Kang Sun, Guoquan Wang, Chenfei Ma: Investigation, Data curation, Writing original draft, Resources. **Lili Liang, Jizhou Wu**: Conceptualization, Methodology, Formal analysis, Funding acquisition. **Dandan Sun Jie Ma**: Writing-review & editing; Validation, Methodology, Investigation, Formal analysis, Supervision, Funding acquisition.

Declaration of Competing Interest

The authors declare that they have no known competing financial interests or personal relationships that could have appeared to influence the work reported in this paper.

Data availability

Data will be made available on request.

Acknowledgments

This work was supported by National Natural Science Foundation of China (62005147, 62175055, 62175140); International Cooperation and Exchange of the National Natural Science Foundation of China (62020106014); Natural Science Foundation of Hebei Province (F2021109003), Science and Technology Research Project of Higher Education of Hebei Province (BJ2021093); Hebei key Laboratory of Optical Fiber Biosensing and Communication Devices (SZX2022010).

References

[1] S. Wang, X. Xu, Y. Sun, J. Liu, H. Li, Heavy metal pollution in coastal areas of South China: a review, Mar. Pollut. Bull. 76 (2013) 7–15, https://doi.org/10.1016/j.marpolbul.2013.08.025.
[2] B. He, Z. Yun, J. Shi, G. Jiang, Research progress of heavy metal pollution in China: sources, analytical methods, status, and toxicity, Chin. Sci. Bull. 58 (2013) 134–140, https://doi.org/10.1007/s11434-012-5541-0.
[3] S. Mitra, A. Chakraborty, A. Tareq, T. Emran, F. Nainu, A. Khusro, A. Idris, M. Khandaker, H. Osman, F. Alhumaydhi, J. Gandara, Impact of heavy metals on the environment and human health: novel therapeutic insights to counter the toxicity, J. King Saud. Univ. Sci. 34 (2022), 101865, https://doi.org/10.1016/j.jksus.2022.101865.
[4] Y. Wang, H. Du, Y. Li, F. Mei, Y. Hu, L. Xiao, J. Ma, S. Jia, Testing universality of Feynman-Tan relation in interacting Bose gases using high-order Bragg spectra, Light. Sci. Appl. 12 (2023) 50, https://doi.org/10.1038/s41377-023-01103-8.
[5] J. Prokisch, B. Kovács, A. Palencsár, I. Szegvári, Z. Győri, Yttrium normalisation: a new tool for detection of chromium contamination in soil samples, Environ. Geochem. Health 22 (2000) 317–323, https://doi.org/10.1023/A:1006799715897.
[6] M. Bergamini, D. Santos, M. Zanoni, Development of a voltammetric sensor for chromium (VI) determination in wastewater sample, Sens. Actuators B Chem. 123 (2007) 902–908, https://doi.org/10.1016/j.snb.2006.10.062.
[7] M. Gondal, M. Dastageer, A. Naqvi, A. Isab, Y. Maganda, Detection of toxic metals (lead and chromium) in talcum powder using laser induced breakdown spectroscopy, Appl. Opt. 51 (2012) 7395–7401, https://doi.org/10.1364/AO.51.007395.
[8] L. Yin, H. Jayan, J. Cai, H. Seedi, Z. Guo, X. Zou, Development of a sensitive SERS method for label-free detection of hexavalent chromium in tea using carbimazole redox reaction, Foods 12 (2023) 2673, https://doi.org/10.3390/foods12142673.
[9] X. Bu, Z. Zhang, L. Zhang, P. Li, J. Wu, H. Zhang, Y. Tian, Highly sensitive SERS determination of chromium (VI) in water based on carbimazole functionalized alginate-protected silver nanoparticles, Sens. Actuators B-Chem. 273 (2018) 1519–1524, https://doi.org/10.1016/j.snb.2018.07.058.
[10] D. Bregnbak, J. Johansen, M. Jellesen, C. Zachariae, J. Thyssen, Chromium (VI) release from leather and metals can be detected with a diphenylcarbazide spot test, Contact Derm. 73 (2023) 281–288, https://doi.org/10.1111/cod.12406.
[11] G. Jung, Y. Kim, H. Lim, Simultaneous determination of chromium (III) and chromium (VI) in aqueous solutions by ion chromatography and

chemiluminescence detection, Anal. Sci. 13 (1997) 463–467, https://doi.org/10.2116/analsci.13.463.
[12] I. Urasa, S. Nam, Direct determination of chromium (III) and chromium (VI) with ion chromatography using direct current plasma emission as element-selective detect, J. Chromatogr. Sci. 27 (1989) 30–37, https://doi.org/10.1093/chromsci/27.1.30.
[13] D. Tai, C. Liu, J. Liu, Facile synthesis of fluorescent carbon dots from shrimp shells and using the carbon dots to detect chromium (VI), Spectrosc. Lett. 52 (2019) 194–199, https://doi.org/10.1080/00387010.2019.1607879.
[14] A. Rovera, A. Tancau, N. Boetti, M. Vedova, P. Maggiore, D. Janner, Fiber optic sensors for harsh and high radiation environments in aerospace applications, Sensors 23 (2023) 2512, https://doi.org/10.3390/s23052512.
[15] L. Wang, Y. Wang, S. Song, F. Li, Overview of fibre optic sensing technology in the field of physical ocean observation, Front. Phys. 9 (2021) 2021, https://doi.org/10.3389/fphy.2021.745487.
[16] E. Castillo, M. Granados, J. Cortina, Chemically facilitated chromium (VI) transport throughout an anion-exchange membrane: application to an optical sensor for chromium (VI) monitoring, J. Chromatogr. A 963 (2002) 205–211, https://doi.org/10.1016/S0021-9673(02)00362-X.
[17] S. Yousefi, F. Shemirani, Selective and sensitive speciation analysis of Cr (VI) and Cr (III) in water samples by fiber optic-linear array detection spectrophotometry after ion pair based-surfactant assisted dispersive liquid-liquid microextraction, J. Hazard. Mater. 254–255 (2013) 134–140, https://doi.org/10.1016/j.jhazmat.2013.03.025.
[18] P. Kishore, M. Shankar, M. Satyanarayana, Detection of trace amounts of chromium (VI) using hydrogel coated Fiber Bragg grating, Sens. Actuators B-Chem. 243 (2017) 626–633, https://doi.org/10.1016/j.snb.2016.12.017.
[19] Y. Long, H. Li, W. Wang, X. Yang, Z. Liu, Ultrasensitive detection of Cr (VI) using a novel SERS optical fiber probe modified by dual-functional methimazole, J. Alloy. Compd. 910 (2022), 164916, https://doi.org/10.1016/j.jallcom.2022.164916.
[20] S. Wankar, U. Alset, R. Gumathannavar, N. Kumbhojkar, A. Kulkarni, Assessment of nano-functionalized cellulosic paper for selective estimation of Cr (VI) using diffuse reflectance spectroscopy, Environ. Pollut. Bioavail. 35 (2023) 1, https://doi.org/10.1080/26395940.2023.2215944.
[21] S. Menon, S. Usha, H. Manoharan, P. Kishore, V. Sai, Metal-organic framework-based fiber optic sensor for chromium (VI) detection, ACS Sens. 8 (2023) 684–693, https://doi.org/10.1021/acssensors.2c02170.
[22] G. Chen, D. Lancaster, T. Monro, Optical microfiber technology for current, temperature, acceleration, acoustic, humidity and ultraviolet light, Sensors, Sensors 18 (2018) 72, https://doi.org/10.3390/s18010072.
[23] Y. Peng, Y. Zhao, M. Chen, F. Xia, Research advances in microfiber humidity sensors, Small 14 (2018), 1800524, https://doi.org/10.1002/smll.201800524.
[24] S. Yap, Y. Chien, R. Tan, A. Alauddin, W. Ji, S. Tjin, K. Yong, An advanced hand-held microfiber-based sensor for ultrasensitive lead ion detection, ACS Sens. 3 (2018) 2506–2512, https://doi.org/10.1021/acssensors.8b01031.
[25] Z. Yi, J. Liu, B. Liu, H. Guo, Q. Wu, J. Shi, X. He, Optical microfiber sensor for detection of Ni^{2+} ions based on ion imprinting technology, Analyst 147 (2022) 358–365, https://doi.org/10.1039/D1AN01982A.
[26] G. Wang, D. Sun, L. Liang, G. Wang, J. Ma, Highly sensitive detection of trace lead ions concentration based on a functional film-enhanced optical microfiber sensor, Opt. Laser Technol. 161 (2023), 109171, https://doi.org/10.1016/j.optlastec.2023.109171.
[27] R. He, C. Teng, S. Kumar, C. Marques, R. Min, Polymer Optical Fiber Liquid Level Sensor: A Review, IEEE Sens. J. 22 (2022) 1081–1091, https://doi.org/10.1109/JSEN.2021.3132098.
[28] P. Xiao, Z. Xu, D. Hu, L. Liang, L. Sun, J. Li, Y. Ran, B.O. Guan, Efficiently Writing Bragg grating in high-birefringence elliptical microfiber for label-free immunosensing with temperature compensation, Adv. Fiber Mater. 3 (2021) 321–330, https://doi.org/10.1007/s42765-021-00087-7.
[29] Y. Ran, Z. Xu, M. Chen, W. Wang, Y. Wu, J. Cai, J. Long, Z. Chen, D. Zhang, B. Guan, Fiber-optic theranostic: interstitial fiber-optic needles for cancer sensing and therapy, Adv. Sci. 9 (2022), 2200456, https://doi.org/10.1002/advs.202200456.
[30] Z. Hou, D. Sun, G. Wang, J. Ma, Highly sensitive cholesterol concentration trace detection based on a microfiber optic-biosensor enhanced specificity with beta-cyclodextrin film, Spectrochim. Acta A Mol. Biomol. Spectrosc. 30 (2023), 122881, https://doi.org/10.1016/j.saa.2023.122881.
[31] C. Zhang, S. Xu, J. Zhao, H. Li, H. Bai, C. Miao, Intensity-modulated refractive index sensor with anti-light source fluctuation based on no-core fiber filter, Opt. Laser Technol. 9 (2017) 358–363, https://doi.org/10.1016/j.optlastec.2017.07.023.
[32] S. Sultan, A kinetic method for the determination of carbimazole in pharmaceutical preparations by oxidation with bichromate in sulfuric acid, Anal. Sci. 8 (1992) 503–506, https://doi.org/10.2116/analsci.8.503.
[33] J. Lou, Y. Wang, L. Tong, Microfiber optical, Sens.: A Rev., Sens. 14 (2014) 5823–5844, https://doi.org/10.3390/s140405823.
[34] Z. Xu, T. Wang, J. Liu, Recent development of polydopamine anti-bacterial naninterfaces, Int. J. Mol. Sci. 23 (2022) 7278, https://doi.org/10.3390/ijms23137278.
[35] M. Alfieri, T. Weil, D. Ng, V. Ball, Polydopamine at biological interfaces, Adv. Colloid Interface Sci. 305 (2022), 102689, https://doi.org/10.1016/j.cis.2022.102689.
[36] T. Saleh, M. Shalalfeh, A. Onawole, A. Saadi, Ultra-trace detection of methimazole by surface-enhanced Raman spectroscopy using gold substrate, Vib. Spectrosc. 90 (2017) 96–103, https://doi.org/10.1016/j.vibspec.2017.03.009.
[37] X. Liao, Y. Chen, M. Qin, Y. Chen, L. Yang, H. Zhang, Y. Tian, Au-Ag-Au double shell nanoparticles-based localized surface plasmon resonance and surface-enhanced Raman scattering biosensor for sensitive detection of 2-mercapto-1-methylimidazole, Talanta 117 (2013) 203–208, https://doi.org/10.1016/j.talanta.2013.08.051.
[38] H. Luo, Q. Sun, X. Li, Z. Yan, Y. Li, D. Liu, L. Zhang, Refractive index sensitivity characteristics near the dispersion turning point of the multimode microfiber-based Mach–Zehnder interferometer, Opt. Lett. 40 (2015) 5042–5045, https://doi.org/10.1364/OL.40.005042.
[39] L. Li, L. Xia, Z. Xie, L. Hao, B. Shuai, D. Liu, In-line fiber Mach-Zehnder interferometer for simultaneous measurement of refractive index and temperature based on thinned fiber, Sens. Actuator A-Phys. 180 (2012) 19–24, https://doi.org/10.1016/j.sna.2012.04.014.
[40] D. Wang, Y. Jiang, X. Geng, B. Yang, L. Li, Study of asymmetric biconical fiber tapers for in-fiber MachZehnder interferometers and applications in singlefrequency fiber lasers, Opt. Express 29 (2021) 14384–14393, https://doi.org/10.1364/OE.419826.
[41] Y. Li, H. Ma, L. Gan, A. Gong, H. Zhang, D. Liu, Q. Sun, Selective and sensitive Escherichia coli detection based on a T4 bacteriophage-immobilized multimode microfiber, J. Biophotonics 11 (2018), e201800012, https://doi.org/10.1002/jbio.201800012.
[42] J. Li, L. Sun, S. Gao, Z. Quan, Y. Chang, Y. Ran, L. Jin, B. Guan, Ultrasensitive refractive-index sensors based on rectangular silica microfibers, Opt. Lett. 15 (2011) 3593–3595, https://doi.org/10.1364/OL.36.003593.
[43] D. Rodriguez, J. Cruz, A. Diez, M. Andres, Coupling between counterpropagating cladding modes in fiber Bragg gratings, Opt. Lett. 36 (2011) 1518–1520, https://doi.org/10.1364/OL.36.001518.
[44] A. Zhang, X. Tao, W. Chung, B. Guan, H. Tam, Cladding-mode-assisted recouplings in concatenated long-period and fiber Bragg gratings, Opt. Lett. 27 (2002) 1214–1216, https://doi.org/10.1364/OL.27.001214.
[45] A. Iadicicco, A. Cusano, A. Cutolo, R. Bernini, M. Giordano, Thinned fiber Bragg gratings as high sensitivity refractive index sensor, IEEE Photon. Technol. Lett. 16 (2004) 1149–1151, https://doi.org/10.1109/LPT.2004.824972.